General features of granular Couette flow and intruder dynamics

2005 J. Phys.: Condens. Matter 17 S2609

(http://iopscience.iop.org/0953-8984/17/24/016)

INSTITUTE OF PHYSICS PUBLISHING JOURNAL OF PHYSICS: CONDENSED MATTER

J. Phys.: Condens. Matter **17** (2005) S2609–S2622 doi:10.1088/0953-8984/17/24/016

General features of granular Couette flow and intruder dynamics

Jian Liu and Anthony D Rosato[1]

Granular Science Laboratory, Department of Mechanical Engineering, New Jersey Institute of Technology, Newark, NJ 07102, USA

E-mail: rosato@adm.njit.edu

Received 16 March 2005
Published 3 June 2005
Online at stacks.iop.org/JPhysCM/17/S2609

Abstract

This paper reports on the behaviour of uniform granular particles of diameter d undergoing a gravity-free shear flow induced through parallel bumpy boundaries that move in opposite directions at constant velocity U. Non-equilibrium, discrete simulations are performed, in which particles are modelled as inelastic, frictional spheres. The flow is described using steady state profiles of mean velocity, granular temperature, solids fraction and normal pressure. A non-uniform local shear rate, characterized by an S-shaped mean velocity profile, produces an imbalance in the contact distribution of particles in the vicinity of the walls so that they drift toward the geometric centre of the flow. A spectral analysis of the transverse velocity provides evidence of convective cell structures in the secondary velocity field whose wavelength decreases with the effective shear rate. A typical tracer particle, whose trajectory has a power spectrum suggestive of persistent fractional Brownian motion, continually samples the entire shear region. In contrast, a large intruder $\phi \equiv D/d > 1$, which also migrates away from energetic regions adjacent to the walls, eventually becomes trapped near the mid-plane of the flow with a speed that increases with ϕ and the effective shear rate $\dot{\varepsilon} = 2U/H$. Fluctuations in the evolution of its transverse velocity component obey a power law of the form $V_y^{\mathrm{rms}} = C\phi^{-a}$, which is a consequence of its greater inertia, while fluctuations in its net force vary directly with ϕ.

(Some figures in this article are in colour only in the electronic version)

1. Introduction

Perhaps one of the most interesting and intriguing features of a granular flow is the phenomenon of segregation, which can be described as the evolution of a well-mixed bulk solid to a spatially non-uniform state. Its occurrence during industrial solids processing and handling operations

[1] Author to whom any correspondence should be addressed.

poses a severe obstacle to the general requirement of creating and maintaining homogeneous mixtures. This inability to achieve and maintain a well-mixed condition of a bulk solid throughout its processing history can lead to serious flaws in the properties of an end product, leading to unfavourable economic consequences [1]. Because of the inherently complex nature of segregation, investigations reported in the literature have focused on identifying controlling mechanisms, such as 'kinetic sieving' [2, 3], shear-induced percolation [4, 5], convection [6–10], local steric effects [11–13], the reverse Brazil nuts effect [14–16] and condensation versus percolation [17].

Solids handling equipment routinely contains moving components in contact with the bulk material to cause material transport; thus it is essential to understand how the boundaries influence the dynamics of the individual particles. A seemingly simple paradigm where boundary interactions play a prominent role is granular Couette flow, in which the material undergoes a non-uniform shear generated by parallel walls that move in opposite directions. Here, flow behaviour is regulated by number of factors, including the ability of the walls to transmit momentum to the granules, the relative width of the sheared layer, the effective shear rate and the distribution of particle properties (i.e., surface friction, restitution coefficient, shape, size and density). For this configuration, numerous investigations on monodisperse systems have been reported in the literature, with studies designed to explore diffusion, slip velocity and wall stresses, force chains and basic rheology (see for example [9, 18–38]). However, investigations on segregation promoted by differences in particle properties in this geometry have not received as much attention.

The first part of this paper reports on the salient features of a fully developed Couette flow which are extracted from soft sphere discrete element simulations. In contrast to the quasi-static regime case (e.g. [18–20, 39–42]), the effective shear rates used in our study generate energetic, collision-dominated flows that are characterized by calculations of the mean field profiles of solids fraction, velocity, granular temperature and pressure. In this, we describe the environment that will be experienced by a single intruder whose properties differ from those of the bulk media. Our study of this aspect is motivated in part by Jenkins and Yoon's [43] steady state kinetic theory-based model for segregation in a thermalized binary mixture under gravity that gives rise to an analytical expression which, in the absence of a temperature gradient, predicts whether an intruder will rise or sink depending on its relative mass and size.

The remainder of this paper is organized as follows. In section 2, we provide an overview of the simulation method, a description of the physical geometry of the Couette model and the relevant parameters chosen for the case studies. Section 3 presents computations of certain mean fields that define the flow, while intruder trajectories and their power spectra are contrasted against a typical tracer particle in the next section. This is followed by a discussion of diffusivity, net force and velocity, as well as the root mean square values of their fluctuations as a function of intruder size. Here, we also separate the effects of particle mass and size to assess which of these factors has the greater impact on its behaviour. Our summary and conclusions are presented in section 6.

2. Simulation method and physical model

We investigate the behaviour of the intruder via discrete element simulations—a method that is credited to Cundall [44] in the 1970s, but actually has its origins in the earlier molecular dynamics computations in the statistical physics community (see for example [45, 46]). The fundamental concept in the discrete element method is the dissipation experienced by macroparticles due to collisions as opposed to energy conservation that characterizes molecular systems. A consequence of the dissipative nature of granular systems is reflected in simulations

that are inherently nonequilibrium with regard to the 'granular temperature'—a measure of fluctuations in particle velocities. Results presented herein represent averages taken in a steady state condition that is attained in only a few seconds (equivalent to approximately 30 collisions per particle per second).

In what follows, we provide a brief description of the force models employed in our code. Complete details can be found in the literature [47–50]. For two colliding spheres, the force along the line of centres (otherwise referred to as the 'normal' direction) consists of loading and unloading paths that are controlled by linear springs of stiffness K_1 and K_2, respectively. Thus, $F_{\text{load}} = K_1\alpha$ and $F_{\text{unload}} = K_2(\alpha - \alpha_0)$, where α denotes the normal penetration with α_0 being its value when $F_{\text{unload}} = 0$. This model produces energy dissipation governed by a constant coefficient of restitution $e = \sqrt{K_1/K_2}$. The force in the tangential plane, which is patterned after Mindlin's [51] theory, features a stiffness that decreases with relative tangential surface displacement until full sliding occurs at the friction limit with coefficient μ. Thus the model incorporates the slip–stick behaviour that takes places in real systems. These soft particles are able to handle flows with enduring contacts, as opposed to standard 'hard' sphere models featured in event-driven simulations [52, 53]. The relatively dense systems considered in our application necessarily admit enduring contacts so that the soft sphere models were seen to be more appropriate. Once the instantaneous forces on all particles have been computed, the system is marched forward in time by numerically solving the equations of motion using a leapfrog algorithm. The integration time step is determined from the approximate duration of the normal force contact mode $\tau = \pi e\sqrt{m/2K_1}$ divided into n steps (typically $n = 30$–40) so that $\Delta t = \tau/n$. For the parameters used in this study, $\Delta t \sim 10^{-6}$ s.

The computational (Couette) cell consists of a rectangular control volume bounded by four periodic sidewalls (see figure 12). The system is driven through collisions transmitted to monodisperse particles (diameter d) by upper and lower, parallel, bumpy walls that move in opposite directions at a constant velocity U. These walls are composed of regular arrays of half-spheres (diameter d) arranged in a tight square configuration. The shear gap H is defined as the distance between the wall bumps, so that the effective shear rate is $\dot{\varepsilon} = 2U/H$. The flow spheres and wall bumps are composed of glass having a mass density $\rho = 2700$ kg m^{-3}, a normal restitution coefficient $e = 0.9$ and a coefficient of sliding friction $\mu = 0.02$. Gravitational acceleration is set to zero since our concern is the influence of the non-uniform shear field on the behaviour of an intruder. We remark that our initial studies showed that the inclusion of a very small amount of gravity caused the system to eventually collapse, resulting in a loss of contact with the upper wall. However, kinetic theory suggests that it is possible to generate a fluid-like 'grain-inertia' flow [2] if $\dot{\varepsilon}^2 d/g$ is sufficiently large.

For the purpose of computing steady state profiles across the shear gap, the cell is partitioned into uniform layers (or strips) whose height is equal to a particle radius. Thus, spatial means in each layer are obtained by averaging through the depth of the flow region (figure 4). Particle fractions are allowed to contribute to mass-weighted layer averages *in lieu* of ascribing the entire particle mass to the layer in which its centre resides. A data point representing the spatial depth-averaged value in the shearing plane is assigned to the middle of a layer. The profile is obtained by fitting straight lines to these data points [54].

Initially, flow spheres are randomly arranged in the cell so that a chosen average (bulk) solids fraction (i.e., the fraction of available volume occupied by solids) ν is obtained. Thereafter, the upper and lower walls move with velocity U in opposite directions. The system quickly attains a steady state after approximately 3–4 s (equivalent to about 90 collisions/particle) so that the flows are fully developed. Statistics used for time averages are gathered after a steady state condition has been attained. However, the system is not in equilibrium in the sense that the temperature profile is not uniform (figure 1(b)).

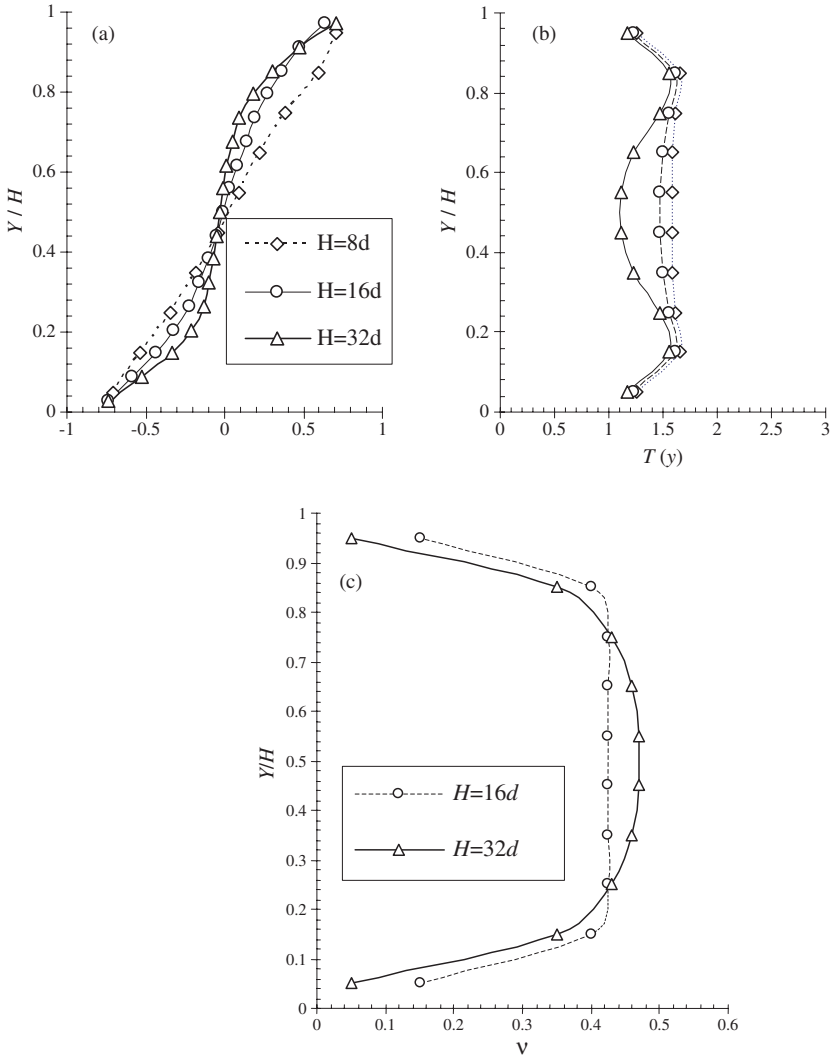

Figure 1. (a) Steady state velocity, (b) granular temperature and (c) solids fraction profiles across the shear gap. Lines are included to show trends in the data.

The flow is characterized by computed steady state profiles across the shear gap of the mean velocity $\bar{u}(y)$, granular temperature $T(y)$, normal pressure P_{yy} and solids fraction $\nu(y)$. The 'granular temperature' describes the mass-averaged kinetic energy associated with the velocity fluctuations, a concept that was proposed by Ogawa [55] as an analogy between the usual thermodynamic temperature and the fluctuating motion of particles in an energetic, collision-dominated granular flow. It is given by

$$T = \frac{\mathbf{u}' \cdot \mathbf{u}'/3}{d^2\dot{\varepsilon}^2} = \frac{(u' \cdot u' + v' \cdot v' + w' \cdot w')/3}{d^2\dot{\varepsilon}^2} \tag{1}$$

where $\mathbf{u}' = (u', v', w')$ are the components of the deviatoric velocity along the coordinate directions and $\dot{\varepsilon} \equiv 2U/H$ is the effective shear rate.

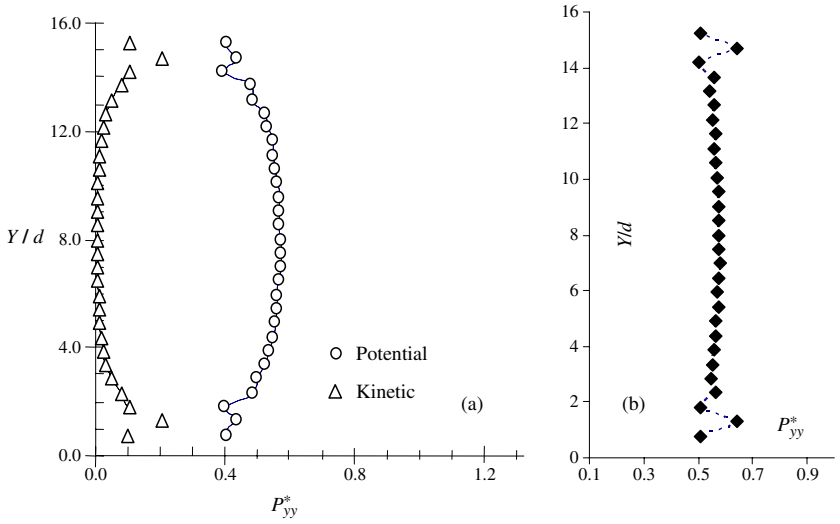

Figure 2. (a) Profile of the kinetic and potential components of the normal pressure for $H/d = 16$. (b) Total normal pressure profile = kinetics + potential.

Granular pressure consists of a kinetic component $\underline{\underline{\mathbf{P}}}^k$ resulting from fluctuations in particle velocities, and a potential component $\underline{\underline{\mathbf{P}}}^c$ due to momentum transfer via collisions. Thus,

$$\underline{\underline{P}} = \underline{\underline{P}}^k + \underline{\underline{P}} = \frac{1}{V}\left[\sum_{i=1}^{N} m_i \mathbf{u}_i' \mathbf{u}_i' + \frac{1}{2}\sum_{i>j}^{N} \mathbf{r}_{ij}\mathbf{F}_{ij}\right] \tag{2}$$

where $\mathbf{r}_{ij}$ is the vector connecting the centres of particles i and j, $\mathbf{F}_{ij}$ is the collision force on particle i due to j and V is the averaging volume. The pressure is normalized in the usual manner [50] by the product of the density, square of the particle diameter and square of the shear rate $\dot{\varepsilon}$, i.e., $\hat{\underline{\underline{\mathbf{P}}}} \equiv \underline{\underline{\mathbf{P}}}/\rho d^2 \dot{\varepsilon}^2$.

3. General features: depth profiles of mean fields

An important trait of the flow is that the velocity and granular temperature profiles are not linear, in contrast to those for a uniform shear condition [50]. A typical steady state (averaged over 100 s) profile of the x component of the normalized velocity $\bar{u}(y)/U$ (figure 1(a)) for the cases $H/d = 8$, 16 and 32 demonstrates that the shear rate is not uniform. The temperature profile (figure 1(b)) has a gradient as it decreases towards the centre of the sheared region, in agreement with the simulation studies of Lun [34]. The largest velocity fluctuations occur near the walls due to the low solids fraction (figure 1(c)) in this region (with a correspondingly higher shear rate), and the presence of the bumps.

The major contributor to the pressure arises from particle collisions rather than velocity fluctuations. The profile of the dimensionless normal pressure P_{yy} in figure 2 for $H/d = 16$ is a mass-weighted spatial average taken over a 100 s time interval. The kinetic contribution, which is largest near the walls where the solids fraction is a minimum, is significantly smaller than the potential part due to the relatively high solids fraction ($\nu = 0.4$) used in this study. The total pressure shown in figure 2(b) is the sum of the kinetic and potential components.

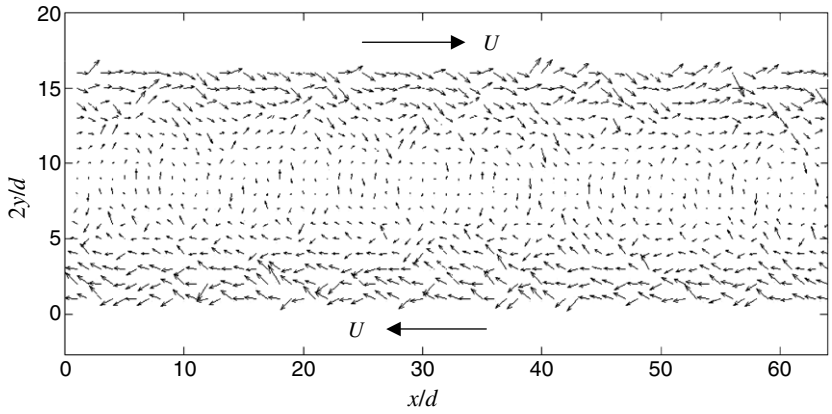

Figure 3. Secondary-velocity-field map $(u'(x, y), v(x, y))$ for the case $U = 8d/s$ and $H/d = 8$, corresponding to $\dot{\varepsilon} = 2/s$.

3.1. Secondary velocity field

Let $u(x, y)$, $v(xy)$ denote the steady state, depth-averaged components of the velocity field in the shearing plane (see figure 4 for a description of the averaging cells). The deviation of $u(x, y)$ from the mean $\bar{u}(y)$ (figure 1(a)) is computed as $u'(x, y) \equiv (u(x, y) - \bar{u}(y))/U$. A typical mapping $(u'(x, y), v(x, y))$ for $U = 8d/s$ and $\dot{\varepsilon} = 2/s$ appears in figure 3. A careful inspection of a sequence of analogous fields produced by varying the effective shear rate $\dot{\varepsilon}$ (for $H/d = 8$) provided evidence of what appeared to be convection cells spanning the length of the flow region having a characteristic wavelength that depends on $\dot{\varepsilon}$. We carried out the following simple analysis of the data to identify these wavelengths. For each $\dot{\varepsilon}$, $v(x, t)$ was constructed by adding the y component of the velocity $v(x, y, t)$ of particles whose centres lie in a slab of length Δx centred at x at time t (as illustrated in figure 4), and then computing its mean $v(x, t)$ by dividing by the number of particles in the slab. The steady state discrete function $v(x)$ is computed from the long time average of $v(x, t)$. The autocorrelation of $v(x)$ was subjected to a spectral analysis to look for the appearance of a dominant wavelength. As an example, figure 5 illustrates the development of $v(x)$ for $\dot{\varepsilon} = 2/s$ to its steady state profile (inset) in a cell having a length $L/d = 64$. A pronounced peak in its autocorrelation function appears at $\lambda \cong 7.5d$ with a power approximately two orders of magnitude larger than those for all other wavelengths. By repeating this procedure for other values of $\dot{\varepsilon}$, we obtained a graph of wavelength versus $\dot{\varepsilon}$, the results of which are given in figure 6. We performed some limited studies for $H/d = 16$ and 32 and at $\dot{\varepsilon} = 1$ and $2/s$. A preliminary analysis of the data suggest a behaviour of the wavelength consistent with that shown in figure 6. At this point, we are unable to provide a clear interpretation of the growth of the wavelength with reduction in shear rate that was found. A more complete study of this phenomenon is planned for future publication.

4. Intruder and tracer particle trajectories

In this section, we discuss the motion of a tracer particle of diameter d and compare it with that of a larger intruder of diameter D in a system having a mean bulk solids fraction $\nu = 0.4$ and $H/d = 16$. At $t = 0$, the intruder particle is positioned adjacent to the lower moving wall. We measure the time T_c for this particle to cross the geometric centre or mid-plane of the cell as a function of the ratio $\phi \equiv D/d$ for several boundary speeds $U = 16, 32, 64\ r/s$ (r is the

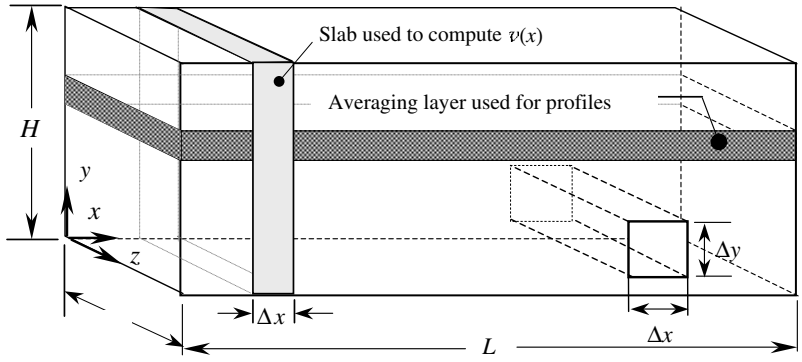

Figure 4. Couette cell depicting averaging volumes used to compute profiles perpendicular to the mean flow, $v(x)$ and $(u'(x, y), v(x, y))$.

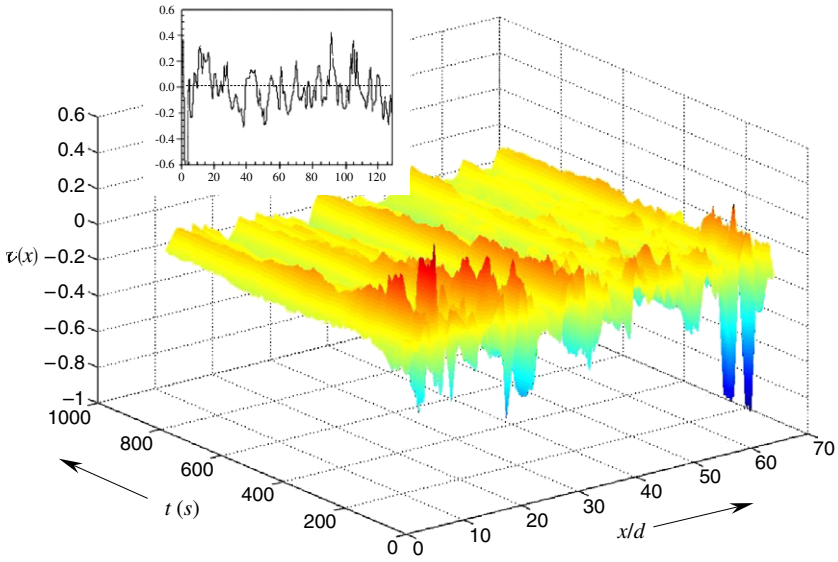

Figure 5. Plot of $v(x)$ as a function of x/d ($L/d = 64$, $\dot{\varepsilon} = 2/s$) showing development to the steady state velocity. This appears in the inset, where the horizontal axis is $2x/d$.

flow particle radius), corresponding to shear rates $\dot{\varepsilon} = 1, 2$ and 4, respectively. The crossing time data are summarized in figure 7(a); the resulting average intruder velocity (figure 7(b)) increases with both shear rate and size ratio.

A tracer or typical flow particle ($\phi = 1$) will visit the entire accessible[2] sheared region over a time interval that depends on the shear rate. Careful observations of flow animations at the relatively high solids fraction used revealed particles jumping between layers formed within the system. A visual inspection of the normalized y-trajectory of a tracer particle in figure 8(a) suggests that there may be a dominant mode. To determine whether this was the case, we computed its power spectral density $P(f) = \lim_{\tau\to\infty}(1/\tau)\hat{Y}(f)\hat{Y}^*(f)$, where τ is the averaging period, $\hat{Y}(f)$ is the fast Fourier transform of the normalized trajectory $Y^*(t)$

[2] The mass centre of a particle is excluded from a small region near the moving walls due to the presence of the bumps.

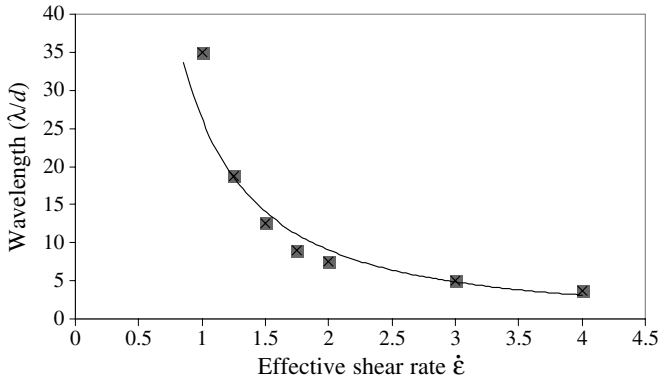

Figure 6. Wavelength λ/d of the convection cells as a function of effective shear rate $\dot{\varepsilon}$ for a fixed shear gap $H/d = 8$. The solid line is included to show the trend.

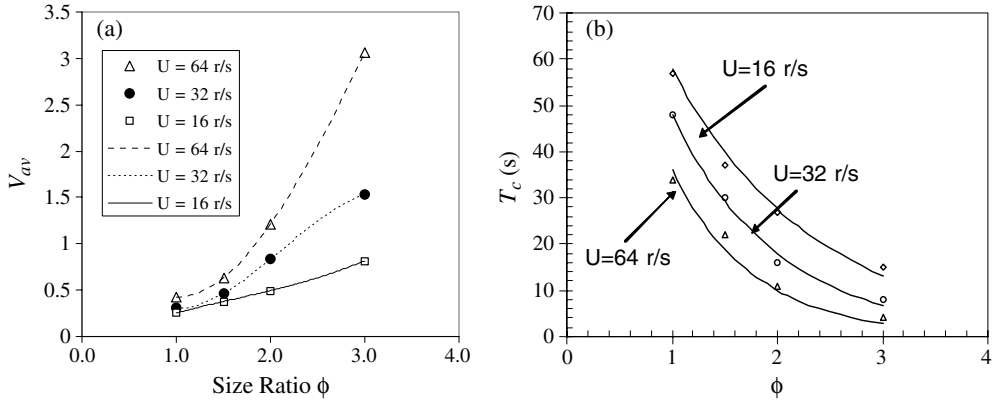

Figure 7. (a) Crossing time T_c (s) versus ϕ at $U = \pm 16, 32, 64\ r/s$; (b) average intruder velocity $V_{av} = S/T_c$, where S is the distance travelled by the mass centre from its initial position near the wall to the mid-plane of the cell.

and $\hat{Y}^*(f)$ is its complex conjugate. We note that normalized y-coordinate Y^* is obtained by rescaling the shear gap distance to account for excluded regions near the walls. If $Y_m(\phi)$ denotes the closest distance possible between the centre of the intruder and the boundary plane, then $Y^* \equiv (Y - Y_m(\phi))/(H - 2 * Y_m(\phi))$. Our analysis of the spectrum in figure 8(b) revealed that $P \propto f^{-2.4}$, which is indicative of a persistent fractional Brownian motion and chaotic dynamics. This conclusion may appear to be somewhat counterintuitive, as one might expect a flow particle traversing across the shear gap to exhibit some periodicity. While we do not completely understand the power spectrum result for the tracer particle, we report it here to promote further discussion. The y-trajectories of intruders of various sizes were analysed in the same manner, i.e., by examining the behaviour of their power spectra P, the results of which are summarized in table 1. After a large intruder reaches the central region of the sheared region (which has a relatively low granular temperature), it is essentially constrained there, an event which we call 'trapping'. This pattern occurred regardless of the intruder's initial location. The phenomenon is reflected in the distributions of Y^* for intruders of various sizes in figure 9. We remark that the affinity of larger particles for the colder (as per the granular temperature) regions of the flow was also found in recent DEM studies [56].

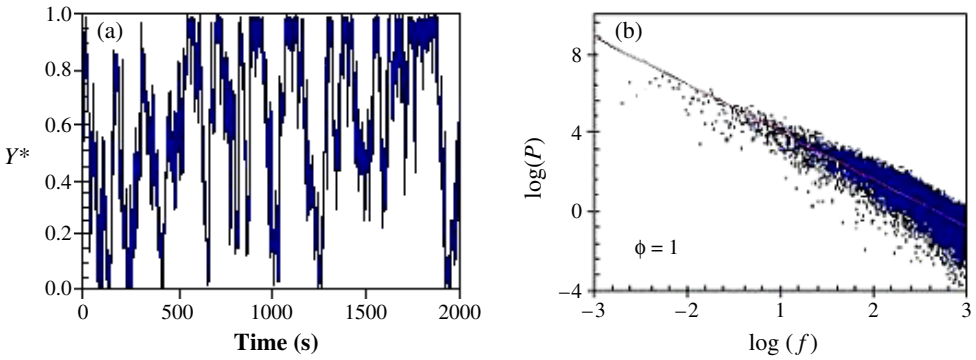

Figure 8. (a) Evolution of the normalized y-trajectory of a tracer particle ($\phi = 1$) and (b) its power spectrum $P \propto f^{-2.4}$ for shear rate $\dot{\varepsilon} = 2/s$ and $U = 16r/s$.

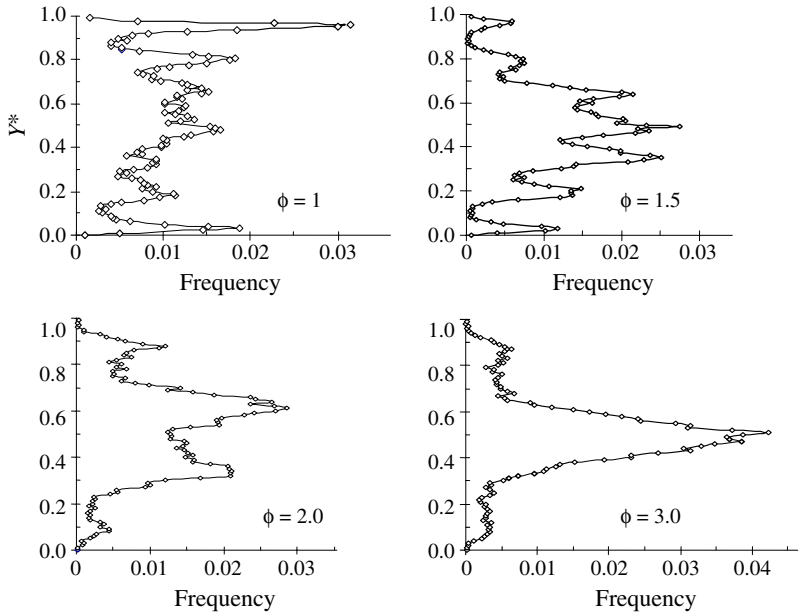

Figure 9. Distribution of the intruder positions along the shear gap for the case $\nu = 0.4$, $\ddot{\varepsilon} = 2$ and $U = 16r/s$.

Table 1. Power spectrum of intruder y-trajectories.

$\phi = D/d$	η	$\beta = -(2\eta + 1)$	$P \propto f^{\beta}$
1.0	0.7	−2.4	$P \propto f^{-2.4}$
2.0	0.9	−2.8	$P \propto f^{-2.8}$
3.0	1.06	−3.0 6	$P \propto f^{-3.06}$

Our results demonstrate that the centreline is a global attractor for the dynamics of intruder particles. We further illustrate this in a binary system in which the large particles occupy 30% of the total particle volume. Initially (at $t = 0$), the large spheres are dispersed throughout the gap region (figures 10(a), 11(a)). However, after only 20 s of flow, the distribution has

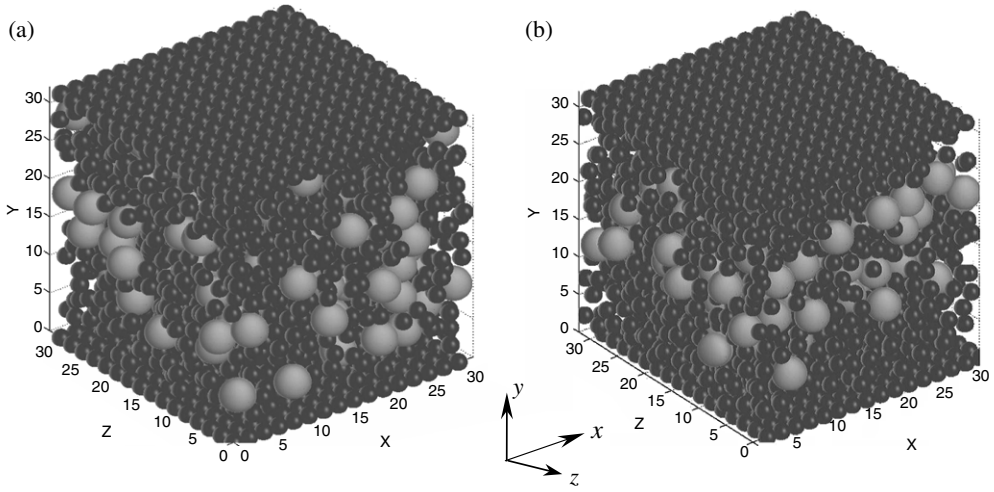

Figure 10. Configuration snapshots at (a) $t = 0$ and (b) at $t = 20$ s.

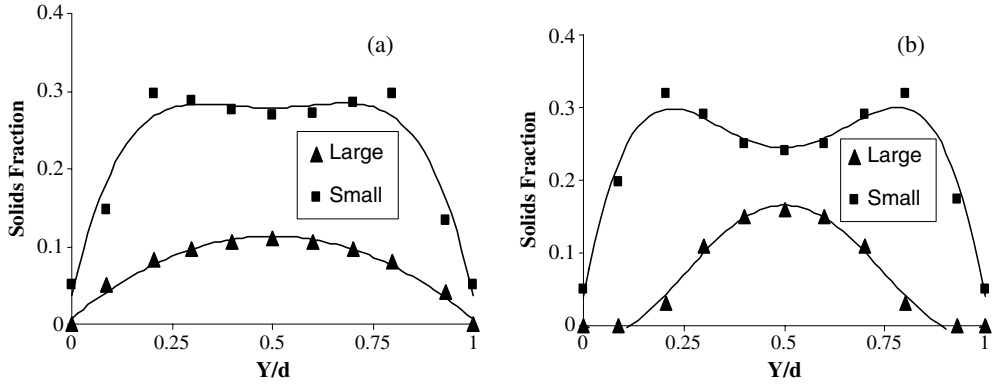

Figure 11. Solid fraction profiles for large and small spheres (a) at $t = 0$ and (b) at $t = 20$ s.

changed so that these particles have migrated towards and remain within a neighbourhood of the centre plane (figures 10(b), 11(b)).

5. Diffusion, velocity and force calculations

There is a general tendency for particles to migrate away from the boundaries towards the centre of the flow region because the local shear rate is greater near the walls. Here, the frequency of collision on the particle's surface facing the wall is larger than on the opposing half. This was verified by calculations that are not shown here. While all particles in the flow experience this imbalance, a large intruder eventually finds that it is unable to return to the walls once it has moved towards the centre, as demonstrated in the previous section. In this section, we highlight differences between the behaviour of a typical flow particle (tracer) and an intruder with regard to diffusivity, velocity and the evolution of the net force acting on each particle. A bulk solids fraction ν of 0.4 was used for these studies. We note that because flow particles and the intruder are assigned the same material density ρ, the results to be presented

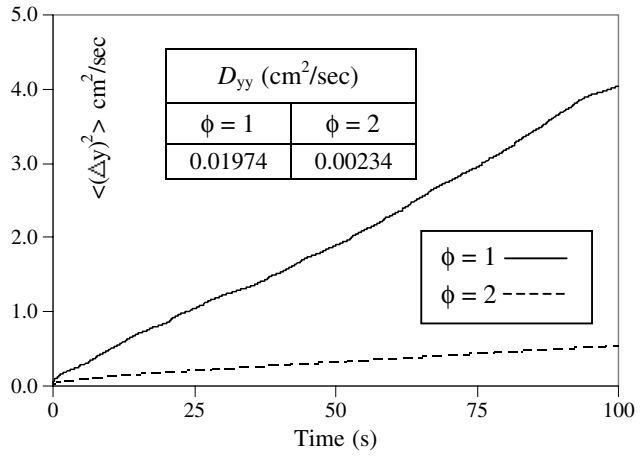

Figure 12. Mean square displacement graph of a tracer ($\phi = 1$) and intruder ($\phi = 2$) for $\dot{\varepsilon} = 4$ and the resulting diffusivities.

reflect the influence of both mass and size. Further on in our discussion, we will examine the contribution of each separately by considering large intruders of the same mass as the flow particles.

The mean square displacement of the y component of the trajectory is computed in the usual manner, i.e.,

$$\langle \Delta y^2 \rangle(t) := \frac{1}{M(t)} \sum_{k=1}^{M(t)} [y_k - y_{k-1}]^2 \tag{3}$$

where $M(t)$ denotes the number of discrete trajectory points at time t. The diffusivity D_{yy} is then found from the limiting slope of the mean square displacement, $D_{yy} = \lim_{t\to\infty} \frac{1}{2t} \langle \Delta y^2 \rangle$, as expected because of the absence of any mean flow in this direction [25]. Effective shear rates $\dot{\varepsilon} = 2, 4$ and 8 were used with size ratios $\phi = 1, 1.5, 2.0$ and 3.0. Our results for $\phi = 1.0$ and 2.0 at $\dot{\varepsilon} = 4$ in figure 12 reveal almost an order of magnitude difference between the diffusivity (cm^2 s^{-1}) of the tracer and an intruder particle. We found this to be the case for intruders of other sizes as well.

Let $N_c(t)$ denote the total number of contacts experienced by the intruder during an interval of time interval Δ that is three orders of magnitude smaller than the timescale over which the dynamics evolves, but much larger than the integration step. The resultant force (time averaged over Δ) acting on this particle perpendicular to the direction of shear is computed as

$$F_y(t)_{\text{net}} = \frac{1}{N_c(t)} \sum_{j=1}^{N_c} F_y^j. \tag{4}$$

Its normalized value is given by $\bar{F}_y(t) \equiv \frac{F_y(t)_{\text{net}}}{\rho(\mathrm{d}^2 U/H)^2}$. Time traces of $\bar{F}_y(t)$ and $\bar{V}_y(t) = V_y(t)/U$ for a typical flow particle and an intruder ($\phi = 3$) are shown in figure 13. In comparison with a tracer, the intruder experiences significantly smaller fluctuations in $\bar{V}_y(t)$, which is simply a consequence of its greater inertia. On the other hand, the fact that $\bar{F}_y(t)$ of the intruder shows a more rapid variation with t and a greater magnitude is principally due to its larger coordination number (i.e., more contacts with the surrounding media).

Steady state, root mean square (rms) values of $\bar{F}_y(t)$ and $\bar{V}_y(t)$, denoted as F_y^{rms}, V_y^{rms}, are presented in figure 14 as a function of ϕ. For $0.5 < \phi < 3.0$, F_y^{rms} increases linearly with ϕ

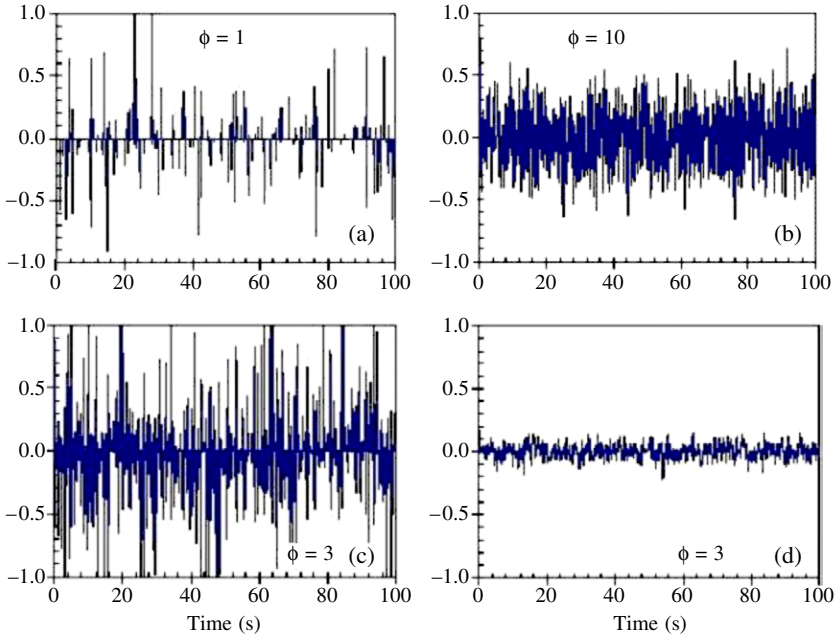

Figure 13. Evolution of $\bar{F}_y(t)$ for (a) $\phi = 1$, (c) $\phi = 3$ and velocity $\bar{V}_y(t)$ for (b) $\phi = 1$ and (d) $\phi = 3$.

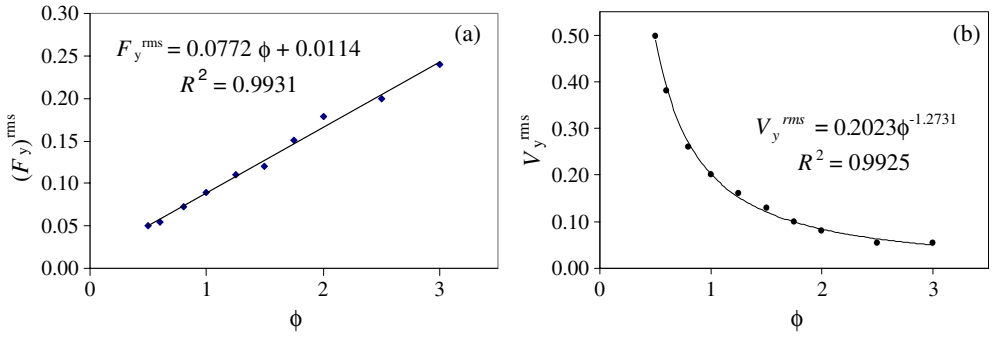

Figure 14. Steady state graphs of $F_y^{\rm rms}$ (a) and $V_y^{\rm rms}$ (b) versus size ϕ. Correlation coefficients R^2 are shown for each fitted curve.

while $V_y^{\rm rms}$ was best fitted to a power law of the form $V_y^{\rm rms} = C\phi^{-a}$. Note that the reduction in $V_y^{\rm rms}$ with ϕ is consistent with its diminished diffusivity D_{yy}.

The decay of $V_y^{\rm rms}$ with ϕ is primarily an inertial effect. This becomes clear if the mass ratio $\phi_m \equiv m_D/m_d$ is varied while keeping $\phi = 1$ so that the intruder diameter is the same as for a flow particle. Note that when the material density of the intruder is equal to that of a flow particle, then $\phi_m = \phi^3$. Figure 15(a) is a graph of $V_y^{\rm rms}$ against ϕ_m with $\phi = 1$, while figure 15(b) illustrates the case when ϕ varies with the material density adjusted so that $\phi_{\rm m} = 1$. These results imply that the intruder's mass has a greater effect on the reduction of $V_y^{\rm rms}$ than does its size relative to the flow particles.

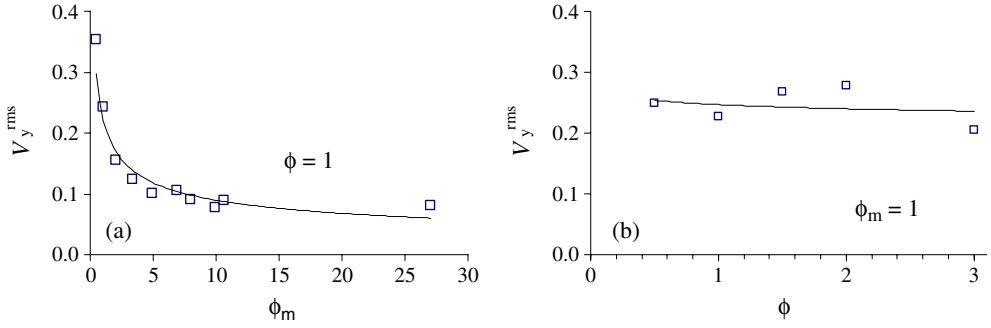

Figure 15. The behaviour of V_y^{rms} for the intruder when (a) its size is equal to that of the flow particle ($\phi = 1$) and its mass is varied, and (b) its mass is constant ($\phi_m = 1$) while its size is varied.

6. Summary and conclusions

We have presented our findings on the behaviour of an intruder within a bed of uniform particles that are sheared between bumpy, parallel walls moving in opposite directions with constant velocity U. Discrete element simulations using soft spheres were carried out to model this flow, which was described by steady state profiles of velocity, solids fraction, granular temperature and normal pressure. Our computations provide evidence of the presence of convection cells across the length of the sheared region having wavelengths that depend on the effective shear rate. As a result of a non-uniform, steady shear rate characterized by an S-shaped velocity profile, particles in the vicinity of the walls slowly migrate towards the centre in such a way as to continually sample the entire accessible flow region. A larger or more massive intruder tends to follow a similar path, but eventually becomes trapped when it reaches the less energetic centre of the flow. Compared with a tracer, it experiences small velocity fluctuations because of its greater inertia, and consequently the motion has a smaller diffusive component.

Acknowledgments

The authors would like to thank O Walton, J Jenkins and D Yoon for helpful discussions. We are also grateful to P Singh for his suggestions of analysing the secondary velocity field, and to D Blackmore for his overall interest in the work.

References

[1] Rosato A D and Blackmore D L (ed) 2000 *IUTAM Symp. on Segregation in Granular Flows* vol 81 (Dordrecht: Kluwer–Academic)
[2] Savage S B and Lun C K K 1988 *J. Fluid Mech.* **189** 311–35
[3] Vallance J and Savage S B 1999 *IUTAM Symp. on Segregation in Granular Flows (Cape, NJ, May 1999)* (Dordrecht: Kluwer–Academic) pp 31–51
[4] Bridgwater J, Foo W S and Stephens D J 1985 *Powder Technol.* **41** 147–58
[5] Bridgwater J 1999 *IUTAM Symp. on Segregation in Granular Flows (Cape, NJ, May 1999)* (Dordrecht: Kluwer–Academic) pp 1–10
[6] Gallas J A C, Herrmann H J and Sokolowski S 1992 *Phys. Rev. Lett.* **69** 1371–3
[7] Gallas J A C, Herrmann H J, Poschel T and Sokolowski S 1996 *J. Stat. Phys.* **82** 443–50
[8] Knight J B, Jaeger H M and Nagel S R 1993 *Phys. Rev. Lett.* **70** 3728–31
[9] Khosropour R, Zirinsky J, Pak H K and Behringer R P 1997 *Phys. Rev.* E **56** 4467–73

[10] Lan Y and Rosato A D 1997 *Phys. Fluids* **9** 3615–24
[11] Duran J, Rajchenbach J and Clement E 1993 *Phys. Rev. Lett.* **70** 2431–4
[12] Jullien R, Meakin P and Pavlovitch A 1992 *Phys. Rev. Lett.* **69** 640
[13] Rosato A D, Strandburg K J, Prinz F and Swendsen R H 1987 *Phys. Rev. Lett.* **58** 1038–42
[14] Ohtsuki T, Kinoshita D and Takemoto Y 1995 *J. Phys. Soc. Japan* **64** 430
[15] Shinbrot T and Muzzio F 1998 *Phys. Rev. Lett.* **81** 4365–8
[16] Shinbrot T and Muzzio F J 2000 *Phys. Today* (March) 25–30
[17] Hong D, C, Quinn P V and Luding S 2001 *Phys. Rev. Lett.* **86** 3423–6
[18] Tardos G I, McNamara s and Talu I 2003 *Powder Technol.* **131** 23–39
[19] Tardos G I, Khan M I and Schaeffer D G 1998 *Phys. Fluids* **10** 335–41
[20] Veje C T, Howell D W and Behringer R P 1999 *Phys. Rev.* E **59** 739–45
[21] Wang C and Tong Z 1998 *Chem. Eng. Sci.* **53** 3803–19
[22] Zamankhan P, Mazouchi A and Sarkomaa P 1997 *Appl. Phys. Lett.* **71** 3790–2
[23] Zamankhan P, Tafreshi H V, Polashenki J W, Sarkomaa P and Hyndman C L 1998 *J. Chem. Phys.* **109** 4487
[24] Zamankhan P, Polashenski J W, Tafreshi J V, Sarkomaa P J and Hyndman C L 1998 *Appl. Phys. Lett.* **73** 450
[25] Campbell C S 1997 *J. Fluid Mech.* **348** 85–101
[26] Conway S L and Glasser B J 2004 *Phys. Fluids* **16** 509–29
[27] Craig K, Buckholz R H and Domoto G 1987 *Trans. ASME J. Tribol.* **109** 232
[28] Hanes D M, Jenkins J T and Richman M W 1988 *J. Appl. Mech.* **110** 969–74
[29] Jenkins J T and Richman M W 1986 *J. Fluid Mech.* **171** 53
[30] Karion A and Hunt M L 2000 *Powder Technol.* **109** 145–63
[31] Louge M Y, Jenkins J T and Hopkins M A 1990 *Phys. Fluids* A **2** 1042–4
[32] Louge M Y, Jenkins J T, Reeves A and Keast S 1999 *Segregation in Granular Flows (Cape May, NJ 1999)* (Dordrecht: Kluwer–Academic) pp 103–12
[33] Lun C K K, Savage S B, Jeffrey D J and Chepurniy N 1984 *J. Fluid Mech.* **140** 223
[34] Lun C K K 1996 *Phys. fluids* **8** 2868–83
[35] Richman M W and Chou C S 1988 *Math. Phys.* **39** 885
[36] Savage S B and Sayed M 1984 *J. Fluid Mech.* **142** 391
[37] Savage S B 1991 *Physics of Granular Media* ed J Dodds and D Bideau (New York: Nova Scientific Publishers) pp 343–62
[38] Savage S B and Dai R 1991 *Advances in Micromechanics of Granular Materials (Potsdam, NY, 1991)* (Amsterdam: Elsevier) pp 151–62
[39] Losert W, Bocquet L, Lubensky T C and Gollub J P 2000 *Phys. Rev. Lett.* **85** 1428–31
[40] Utter B and Behringer R P 2004 *Phys. Rev.* E **69** 031308-1–12 (*Preprint* cond-mat/0309040)
[41] Radjai F 2002 *Phys. Rev. Lett.* **89** 064302
[42] Fenistein D, Meent J W V d and Hecke M v 2004 *Phys. Rev. Lett.* **92** 094301
[43] Jenkins J T and Yoon D K 2002 *Phys. Rev. Lett.* **88** 194301
[44] Cundall P A 1974 Rational design of tunnel supports: a computer model for rock-mass behavior using interactive graphics for input and output of geometrical data *Report No. Technical Report MRD*
[45] Ashurst W T and Hoover W G 1973 *Phys. Rev. Lett.* **31** 206–9
[46] Alder B J and Wainwright T E 1956 *Proc. Int. Union of Pure and Applied Physics (Brussels, 1956)*
[47] Walton O R 1992 *Particulate Two-Phase Flow* ed M C Roco (Boston, MA: Butterworths) pp 884–911
[48] Walton O R and Braun R L 1986 *J. Rheol.* **30** 949–80
[49] Walton O R *Second U.S.–Japan Seminar on Micromechanics of Granular Materials (Potsdam, NY, 1991)* (Amsterdam: Elsevier) pp 453–61
[50] Walton O R and Braun R L 1986 *Acta Mech.* **63** 73–86
[51] Mindlin R D and Deresiewicz H 1953 *J. Appl. Mech.* **20** 327
[52] Luding S 1995 *Phys. Rev.* E **52** 4442–57
[53] Luding S 1994 *Dissertation Thesis* Albert-Ludwigs-Universitat
[54] Rosato A D and Kim H J 1994 *Contin. Mech. Thermodyn.* **6** 1–20
[55] Ogawa S 1978 *U.S.–Japan Seminar on Continuum Mechanical and Statistical Approaches in the Mechanics of Granular Materials (Sendai, Japan, 1978)* Gakujutsu Bunken Fukyu-Kai, pp 208–17
[56] Dahl S R and Hrenya C M 2004 *Phys. Fluids* **16** 1–12